Available online at www.sciencedirect.com
SCIENCE DIRECT
Journal of Photochemistry and Photobiology A: Chemistry 172 (2005) 81–88
Journal of Photochemistry and Photobiology A:Chemistry
www.elsevier.com/locate/jphotochem

# Physicochemical and photocatalytic characterizations of $TiO_2$/Pt nanocomposites

Zhaolin Liu[a,*], Bing Guo[a], Liang Hong[a,b], Huixin Jiang[a]

[a] *Institute of Materials Research and Engineering of Singapore, MPMC, 3 Research Link, Singapore 117602, Singapore*
[b] *Department of Chemical and Environmental Engineering, National University of Singapore, 10 Kent Ridge Crescent, Singapore 119260, Singapore*

Received 20 August 2004; received in revised form 28 October 2004; accepted 18 November 2004
Available online 4 January 2005

**Abstract**

Spherical and uniform Pt nanoparticles with sizes of 2–6 nm have been formed on $TiO_2$ nanoparticles and nanowires by microwave irradiation and exhibited very high photocatalytic activity in the decomposition of methyl orange. X-ray photoelectron spectroscopy (XPS) analysis revealed that the $TiO_2$/Pt composites contained mostly Pt(0), with traces of Pt(II) and Pt(IV). These results indicate that nanoparticles of platinum were formed on the surface of $TiO_2$ nanoparticles and nanowire. X-ray diffraction (XRD) showed that $TiO_2$/Pt composites only displayed the characteristic diffraction peaks of a $TiO_2$ anatase structure. $TiO_2$/Pt composites exhibited very high photocatalytic activities in the decomposition of methyl orange.


*Keywords:* $TiO_2$; Nanoparticles; Nanowires; Platinisation; Photodegradation

## 1. Introduction

Among the various semiconductor photocatalysts (i.e., ZnO, ZnS, CdS, $Fe_2O_3$, $WO_3$ etc.) titanium dioxide ($TiO_2$) has been most actively investigated owing to its photostability, strong oxidizing power, non-toxicity, chemical and biological inertness and stability, and low cost. Due to these advantages, $TiO_2$ has attracted considerable attention as the photocatalyst in various processes, such as deodour of drinking water, degradation of oil spills in water systems, and decomposition of harmful organic contaminants, e.g. herbicides, pesticides, and refractive dyes. In order to improve photocatalytic efficiency, tremendous efforts have been devoted in recent years, which also include synthesis of composite photocatalysts [1–4] and $TiO_2$ nanowires (TNW) [5–7]. Doping $TiO_2$ by certain types of transition metals has been extensively studied since these transition metal clusters could elongate electron–hole pair separation [8,9]. In particular, Pt-deposited $TiO_2$ has been frequently used in a variety of photoreactions, and the same system was also reported to speed up the water splitting reaction [10,11] and oxidation of organic compounds [12–14] and CO [15]. However, the mechanism which deposition of Pt on $TiO_2$ greatly enhances the photocatalytic oxidation reactions was not well clarified. Role of metal nanoparticles in $TiO_2$/Pt nanocomposite was seldom discussed.

The polyol process, in which an ethylene glycol solution of the metal precursor salt is slowly heated to produce colloidal metal, has recently been extended to produce metal nanoparticles supported on carbon and $Al_2O_3$ [16–18]. In the process the polyol solution containing the metal salt is refluxed at 393–443 K to decompose ethylene glycol to yield in situ generated reducing species for the reduction of the metal ions to their elemental states. The fine metal particles produced as such may additionally be captured by a support material suspending in the solution. Conductive heating is often used but microwave dielectric loss heating may be a better synthesis option in view of its energy efficiency, speed, uniformity, and implementation simplicity [19]. In this paper,

* Corresponding author. Tel.: +65 68727532; fax: +65 68720785.
*E-mail address:* zl-liu@imre.a-star.edu.sg (Z. Liu).

1010-6030/$ – see front matter © 2004 Elsevier B.V. All rights reserved.
doi:10.1016/j.jphotochem.2004.11.008

a simple microwave-assisted polyol procedure for preparing Pt nanoparticles supported on $TiO_2$ powder (TP) or $TiO_2$ nanowire is reported. In addition, the adsorption equilibrium constants and the kinetic constants of methyl orange photocatalytic oxidation in aqueous suspensions for various catalysts prepared were also investigated. A possible mechanism of platinised $TiO_2$ with higher photocatalytic activities is also discussed.

## 2. Experimental

### 2.1. Chemicals

Analytic grades of titanium isopropoxide (TIPO: $Ti[OCH(CH_3)_2]_4$), isopropyl alcohol, hydrogen hexachloroplatinate hydrate (Aldrich, A.C.S. Reagent), sodium hydroxide, ethylene glycol (EG) (Mallinckrodt, AR), chloride acid, nitric acid, and methyl orange were used for the synthesis and test. All aqueous solutions were prepared using distilled water.

### 2.2. Preparation of $TiO_2$ powder and $TiO_2$ nanowire

A solution consisting of 30 mL of $Ti[OCH(CH_3)_2]_4$ and 5 mL of isopropyl alcohol was added dropwise (1 mL/min) into 180 mL of distilled water at pH 1.5 (adjusted with $HNO_3$). The resulting solution was continuously stirred for 10–12 h until a transparent colloid was formed. The colloid solution was concentrated at 35–40 °C with a rotary evaporator and then calcined at 550 °C for 2 h in air to yield a $TiO_2$ powder.

Single crystalline anatase $TiO_2$ nanowire was synthesized in a simple hydrothermal setup using the method similar to that described by Kasuga et al. [5]. In a typical preparation system, 1 g of $TiO_2$ powder was placed in a Teflon-lined autoclave of 50 mL capacity. The autoclave was filled with 10 M NaOH aqueous solution up to 80% of its total volume, then sealed in a stainless steel tank and maintained at 200 °C for 24 h. After the autoclave was naturally cooled to room temperature, the specimen obtained was sequentially washed with dilute HCl aqueous solution, distilled water and absolute ethanol for several times, and dried at 70 °C for 5 h.

### 2.3. Preparation of TP/Pt and TNW/Pt composites

In a 50 mL beaker, 1.03 mL of an aqueous solution of 2 mM $H_2PtCl_6{\cdot}6H_2O$ was mixed with 25 mL of ethylene glycol, 0.5 mL of 0.4 M NaOH was added dropwise into the resulting solution. After this, 0.040 g of the as-prepared $TiO_2$ powder or $TiO_2$ nanowire were added to the mixture and sonicated. The beaker and its contents were heated in a microwave oven (National NN-S327WF, 2450 MHz, 700 W) for 50 s. The resulting suspension was filtered; and the residue was washed with acetone and dried at 100 °C over night in a vacuum oven. $TiO_2$ powder/Pt (TP/Pt) and $TiO_2$ nanowire/Pt (TNW/Pt) composites with amount of Pt 1 wt.% were obtained.

### 2.4. Characterization

The surface morphology of the $TiO_2$ nanowire was recorded on a JSM 6700 field emission gun scanning electron microscope (FEG-SEM) with an accelerating voltage of 5 kV. The size and morphologies of $TiO_2$ and $TiO_2$/Pt composites were characterized by TEM imaging (JEOL JEM 2010). The Pt contents were determined by EDX (JEOL JSM-5600LV). Samples were first ultrasonicated in acetone for 1 h and then deposited on 3 mm Cu grids covered with a continuous film of carbon. The actual platinum contents in the TP/Pt and TNW/Pt were determined by inductively coupled plasma spectroscopy (ICP). Crystalline structures of the powders were characterized by X-ray diffraction (XRD) on a Bruker GADDS diffractometer using Cu Kα radiation and a graphite monochromator (the accelerating voltage and the applied current were 40 kV and 40 mA, respectively). X-ray photoelectron spectroscopy (XPS) analyses of the samples were performed on a VG ESCALAB MKII spectrometer. Narrow scan photoelectron spectra of Ti 2p, O 1s and Pt 4f were recorded. Peak deconvolution was performed using the curve-fitting program VGX900.

### 2.5. Adsorption experiment

To determine the adsorption property of $TiO_2$ and $TiO_2$/Pt composites, adsorption isotherm tests were preformed in the dark. 100 mg of $TiO_2$ or $TiO_2$/Pt composites was added in 100 ml of methyl orange solutions with different initial concentrations and then stirred at 200 rpm for 24 h at 25 °C. The methyl orange concentrations in the $TiO_2$ or $TiO_2$/Pt suspensions before and after the adsorption tests were analyzed to determine the adsorbed amount of methyl orange on the catalysts through a mass balance.

### 2.6. Photon-irradiation experiment

The light source used for the photocatalytic experiment consists of 10 photochemical lamps (each with 30 W) having maximum output at wavelength of 300 nm. The experiments were conducted in a Rayonet photochemical reactor equipped with the above lamps. The suspensions were prepared by adding 100 mg of photocatalyst powder into 100 mL of methyl orange aqueous solution ($C_0$ = 0.21 mM). Prior to photooxidation, the suspension was magnetically stirred in the dark for 1 h to establish adsorption/desorption equilibrium. The aqueous suspensions containing methyl orange and catalysts were irradiated under the UV lamp. At the given time intervals, the analytical samples were taken from the suspension and immediately centrifuged and filtered to remove the particles. The filtrates were characterized by Shimadzu UV-2101PC spectroscopy.

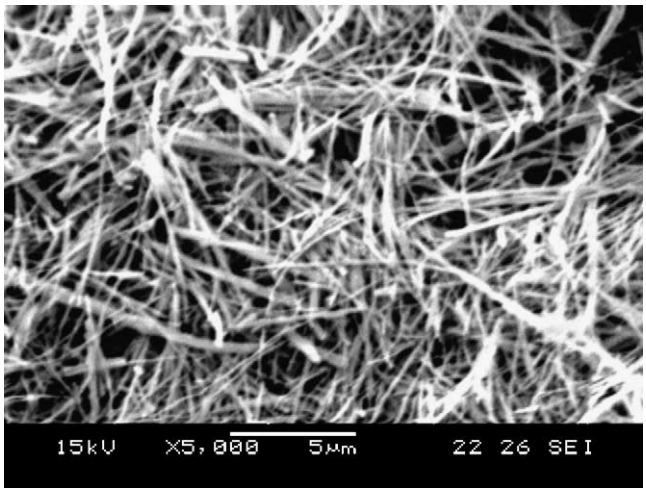


Fig. 1. SEM image of anatase $TiO_2$ nanowire.

## 3. Results and discussion

### 3.1. Characterization of Pt nanoparticles on $TiO_2$

Fig. 1 showed a typical SEM image of the single crystalline anatase $TiO_2$ nanowires of as-prepared $TiO_2$ nanowires. The SEM image indicated the nanowires are quite clean with no contamination attached to their surface. Some of the nanowires aggregated into bundles which might happen while the reaction or the preparation of SEM sample. This explains why some of the nanowires are looked wider than others. Fig. 2a and c showed typical TEM images of an isolated $TiO_2$ nanowire and the $TiO_2$ powder. The results as shown in Fig. 2c indicated that $TiO_2$ powder was aggregated. The average particle size of the individual particle was about 20 nm or even smaller and it seems that most of the fine particles were in round shape. Wire-shaped product with the diameter about 100 nm was observed.

In our approach, platinum nanoparticles is prepared and directed deposited on the $TiO_2$ surface by microwave heating of EG solutions of platinum salt. The sizes of the platinum particles were analyzed by TEM.

Fig. 2c and d are typical TEM images of TP/Pt and TNW/Pt catalysts, showing a remarkably uniform and high dispersion of metal particles on the $TiO_2$ surface. The particle size distributions of the metal in the supported catalysts were obtained by directly measuring the size of 150 randomly chosen particles in the magnified TEM images (e.g. Fig. 2e for the TP/Pt and Fig. 2f for the TNW/Pt). The average diameters of $3.9 \pm 0.3$ nm for TP/Pt and $3.7 \pm 0.3$ nm for TNW/Pt were accompanied by relatively narrow particle size distributions (2–6 nm). This is similar to our previous results to prepare Vulcan carbon and carbon nanotubes supported PtRu particles by a microwave-assisted polyol process [16,17]. The microwave assisted heating of $H_2PtCl_6/NaOH/H_2O$ in ethylene glycol had evidently facilitated the formation of smaller and more uniform Pt particles and their dispersion on either the $TiO_2$ powder or $TiO_2$ nanowire surface. It is generally agreed that the size of metal nanoparticles is determined by the rate of reduction of the metal precursor. The dielectric constant (41.4 at 298 K) and the dielectric loss of ethylene glycol are high, and hence rapid heating occurs easily under microwave irradiation. In ethylene glycol mediated reactions (the 'polyol' process) ethylene glycol also acts as a reducing agent to reduce the metal ion to metal powders. The fast heating by microwave accelerates the reduction of the metal precursor and the nucleation of the metal clusters. The easing of the nucleation limited process greatly assists in small particle formation. Additionally, the homogeneous microwave heating of liquid samples reduces the temperature and concentration gradients in the reaction medium, thus providing a more uniform environment for the nucleation and growth of metal particles. The $TiO_2$ surface may contain sites suitable for heterogeneous nucleation and the presence of a $TiO_2$ surface interrupts particle growth. The smaller and nearly single dispersed Pt nanoparticles on $TiO_2$ prepared by microwave irradiation can be rationalized in terms of these general principles.

ICP measurements showed Pt contents of 0.93 wt.% for TP/Pt and 0.88 wt.% for TNW/Pt prepared from the feeds of 1 wt.%.

XRD is a bulk analysis that reveals the crystal structure, lattice constants, and crystal orientation of the $TiO_2$ and $TiO_2$ composites. $TiO_2$ mainly exists in three crystallographic forms, anatase, brookite, and rutile. Anatase has been found, in most of the cases, to be photocatalytically more active than rutile. And rutile was thermodynamically more stable than anatase. Brookite was the unstable phase of $TiO_2$. The XRD peaks at $2\theta = 25.25^\circ$ and $48.0^\circ$ in the spectrum of $TiO_2$ are easily identified as the anatase form, whereas the XRD peaks at $2\theta = 27.42^\circ$ and $54.5^\circ$ belong to the rutile form. The powder X-ray diffraction patterns for TP/Pt and TNW/Pt are shown in Fig. 3 alongside the diffraction patterns of $TiO_2$ powder and TNW used as a comparison. All the relatively sharp peaks could be indexed as anatase $TiO_2$, which are basically in agreement with the reported values (JCPDS no. 21-1272). Additionally, no peaks from platinum ($40.0^\circ$ and $68.1^\circ$) were observed for TP/Pt and TNW/Pt, which may be Pt loadings of 1 wt.% only. No characteristic peaks of other impurities, such as NaCl and $Na_2TiO_3$, were observed for TNW and TNW/Pt, which indicate that the TNW has high purity.

The average crystallite size (diameter) $L$ of $TiO_2$ nanoparticles can be estimated from the integral width of the diffraction peaks using the Scherrer formula with their (1 0 1) peaks: $L = K\lambda/\beta \cos\theta$, where $K$ is the shape factor (a value of 0.9 was used in this study), $\lambda$ the X-ray radiation wavelength (1.54056 Å for Cu K$\alpha$), and $\beta$ is the line width at half-maximum height of the main broadening. The calculation results, which are 22.4 nm and 21.65 nm for $TiO_2$ powder and TP/Pt, show that the average crystalline size of the anatase phase did not changed with platinum nanoparticles deposited

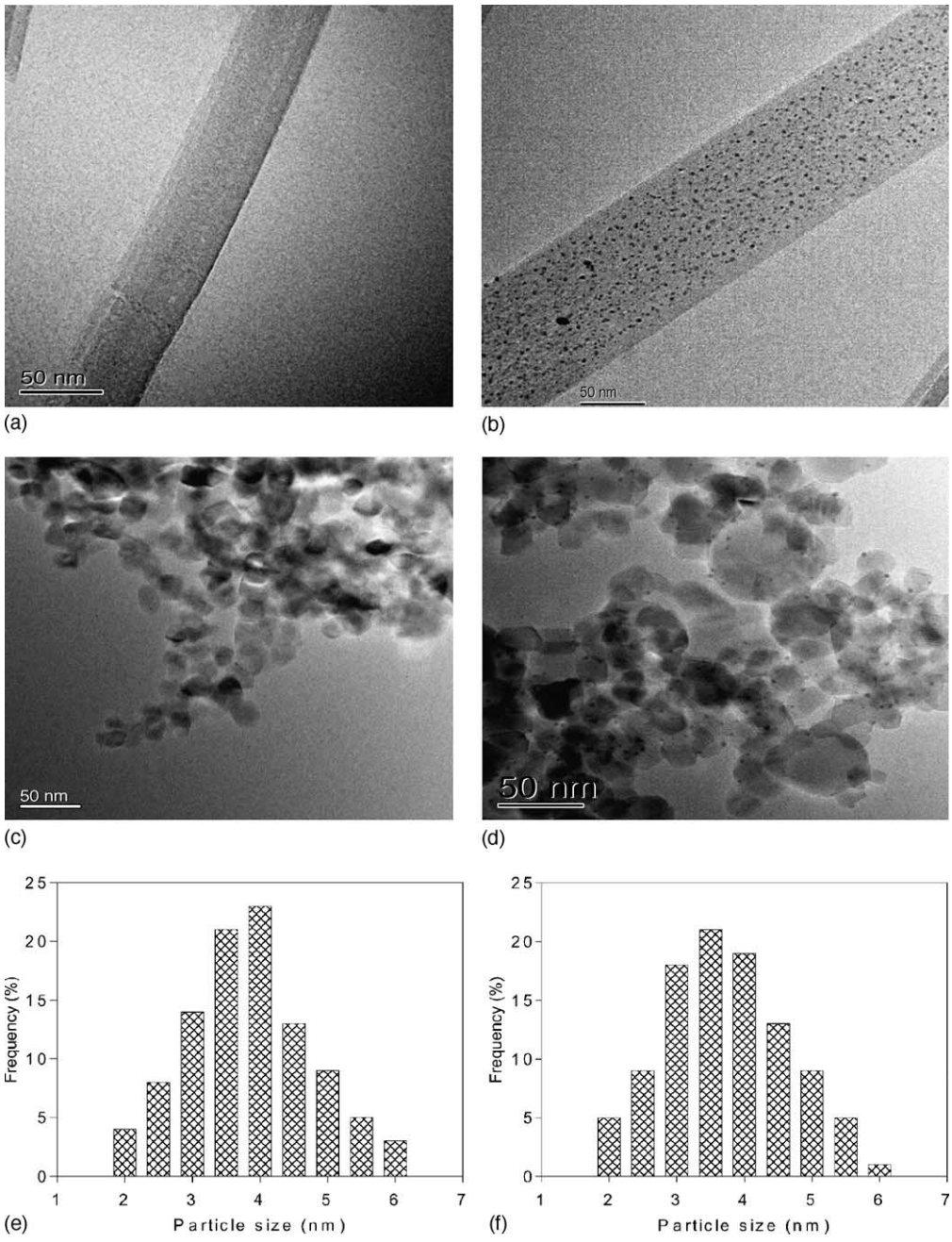


Fig. 2. TEM image of TP (a), $TiO_2$ nanowire (b), microwave-synthesized TP/Pt (c) and TNW/Pt (d) catalysts (Pt loading, 1 wt.%). Histograms of particle size distributions TP/Pt catalyst (e) and TNW/Pt (f).

on $TiO_2$ surfaces. The results are in good agreement with the TEM measurements.

According to XPS investigation, the electron-binding energies of the main peaks pertaining to Ti 2p, O 1s, and Pt 4f were summarized in Table 1; they agree well with the values reported in the literature [20–22]. Fig. 4 shows the Ti 2p, O 1s, and Pt 4f regions of the XPS spectrum of the TNW/Pt composite. From the XPS spectrum of the Ti 2p, the spin–orbit components ($2p_{3/2}$ and $2p_{1/2}$) of the peak were well deconvoluted by two curves (at approximately 458.7 eV and 464.3 eV, respectively) indicating that the Ti element mainly existed as the chemical state of $Ti^{4+}$ on the basis of the principle and instrument handbook of XPS [23]. These agree well with the values reported in the literature [24,25]. It seems that the Pt nanoparticles inserting did not affect the peak position of Ti 2p much from Table 1.

The XPS spectra of O 1s in the figure was asymmetric, the left side was wider than the right from the figure, indicating that at least two kinds of oxygen species were present at the surface, which can be recognized by resolving XPS curves. The dominant peak at about 530 eV was characteristic of metallic oxides, which was in agreement with O 1s

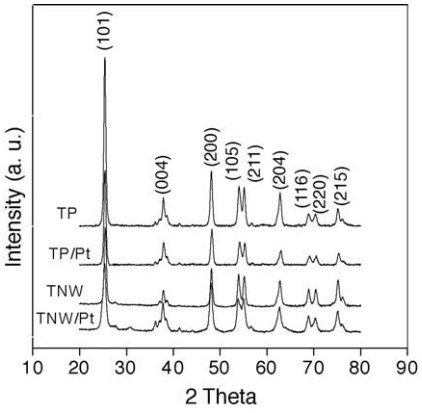


Fig. 3. XRD patterns of the $TiO_2$ and $TiO_2$/Pt nanocomposites.

electron-binding energy arising from titania lattice. The oxygen atoms in the titania matrix make the primary contribution to the spectrum. Another O 1s peak at 532 eV was due to surface hydroxyl.

The Pt 4f signal consisted of three pairs of doublets. The most intense doublet (71.0 eV and 74.3 eV) was due to metallic Pt. The second set of doublets (72.4 eV and 75.7 eV), which was observed at BE 1.4 eV higher than Pt(0), could be assigned to the Pt(II) chemical state as in PtO and $Pt(OH)_2$ [26]. The third doublet of Pt was the weakest in intensity and occurred at even higher BEs (74.2 eV and 77.7 eV). These are the indications that they were most likely caused by a small amount of Pt(IV) species on the surface. The slight shift in the Pt(0) peak to higher binding energies is a known effect for small particles, as has been reported by Roth et al. [27].

### 3.2. Photodegradation of dye

The generally accepted first steps in photocatalytic processes are

$$TiO_2 + h\nu \rightarrow TiO_2(h^+) + e^- \quad (1)$$

$$TiO_2(h^+) + H_2O(ads) \rightarrow HO^{\bullet} + H^+ + TiO_2 \quad (2)$$

In the presence of adsorb oxygen, the cathodic process will be the $O_2$ reduction by conduction band electrons, which can also result in the formation of hydroxyl radicals.

$$e^- + O_2(ads) \rightarrow O_2^{\bullet -} \quad (3)$$

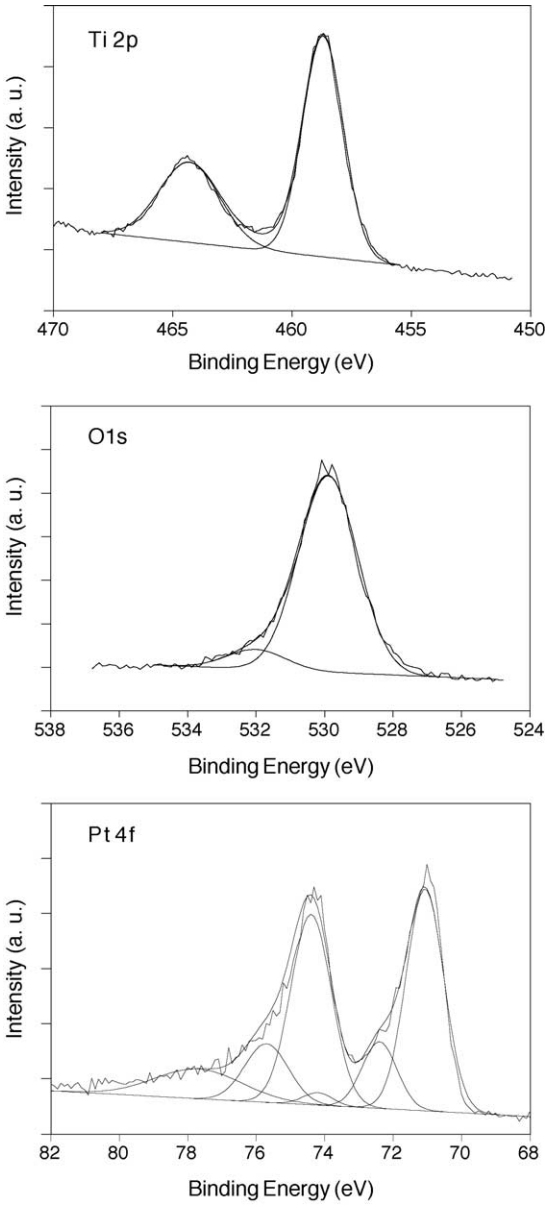


Fig. 4. X-ray photoelectron spectra of the TNW/Pt nanocomposite.

$$O_2^{\bullet -} + 2H^+ + e^- \rightarrow H_2O_2 \quad (4)$$

$$H_2O_2 + e^- \rightarrow HO^{\bullet} + OH^- \quad (5)$$

Table 1
XPS binding energy values of $TiO_2$ and $TiO_2$/Pt composites

| Photocatalysts | Binding energy (eV) | | | | | |
|---|---|---|---|---|---|---|
| | Ti $2p_{3/2}$ | Ti $2p_{1/2}$ | Pt $4f_{7/2}$ | Pt $4f_{5/2}$ | O 1s($O_{lattice}$) | O 1s($OH^-$) |
| TP | 458.4 | 464.5 | – | – | 529.8 | 532.0 |
| TNW | 458.2 | 464.2 | – | – | 529.7 | 531.8 |
| TP/Pt | 458.4 | 464.3 | 71.2 | 74.5 | 530.1 | 531.9 |
| TNW/Pt | 458.7 | 464.3 | 71.0 | 74.3 | 530.0 | 532.0 |

The main reactions of the photocatalytic degradation of methyl orange have been suggested to be schematically represented by the following scheme [28]:

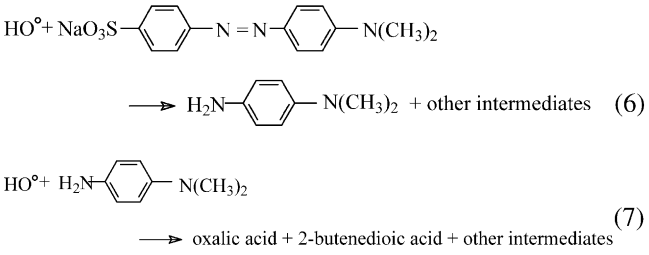


$$h^{+}(HO^{\bullet}) + \text{oxalic acid} + \text{2-butenedioic acid} \rightarrow CO_2 + H_2O \quad (8)$$

The photocatalytic degradation of methyl orange under UV irradiation proceeded with the cleavage of the azo-bond, generating 4-dimethylamino aniline, and then underwent a further opening of the phenyl-rings to form small molecular compounds such as oxalic acid and 2-butenedioic acid, which readily decomposes irreversibly liberating $CO_2$.

Fig. 5 shows the absorption spectra of the 10 times diluted of centrifuged slurry samples taken from the photocatalytic reactor after various times of UV exposure for the $TiO_2$ powder sample. Methyl orange has the maximum UV absorption at 460 nm; i.e., the initial absorbance of a 0.02 mM solution of methyl orange before decomposition was 0.55. The absorbance at 460 nm is significantly lowered with times of UV exposure. The change of methyl orange concentration as a function of duration of UV exposure is compared in Fig. 6. The experimental results demonstrated that the platinised $TiO_2$ catalysts (TP/Pt and TNW/Pt) achieved faster methyl orange photodegradation rates than the pure $TiO_2$ catalysts (TP and TNW) significantly. The photocatlytic activity of the $TiO_2$ materials can be related to their different physicochemical properties. Platinisation increased the photocatalytic efficiency in two cases, no matter were the type of catalyst.

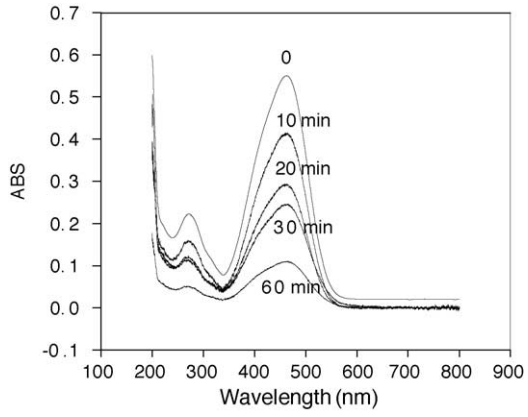


Fig. 5. The absorption spectra of the 10 times diluted centrifuged slurry samples taken from the photocatalytic reactor after various times of UV exposure for the $TiO_2$ powder sample.

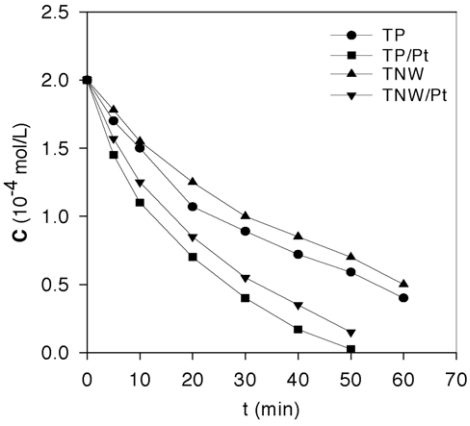


Fig. 6. The change of methyl orange concentration as a function of duration of UV exposure on the different catalysts.

To study the kinetics of the heterogeneous photocatalytic degradation in $TiO_2$ suspensions, some researchers addressed that the kinetics in these aqueous suspensions should be described based on both the substrate concentration in the bulk solution and also the substrate amount absorbed on the photocatalysts [29,30]. A set of adsorption tests was carried out in the dark and the methyl orange adsorption isotherms on the different catalysts by plotting $C/\Gamma$ versus $C$ are shown in Fig. 7, which were well fitted by Langmuir adsorption model [31] as follows:

$$\frac{C}{\Gamma} = \frac{C}{\Gamma_{max}} \frac{1}{(K_a \Gamma_{max})} \quad (9)$$

where $C$ is the equilibrium concentration of the substrate in the solution in mole, $K_a$ the adsorption equilibrium constant in L/mol, and $\Gamma_{max}$ is saturated adsorption capacity in mol/g.

The values of $\Gamma_{max}$ and $K_a$ were obtained from the above fitting and are listed in Table 2. The results indicated that the

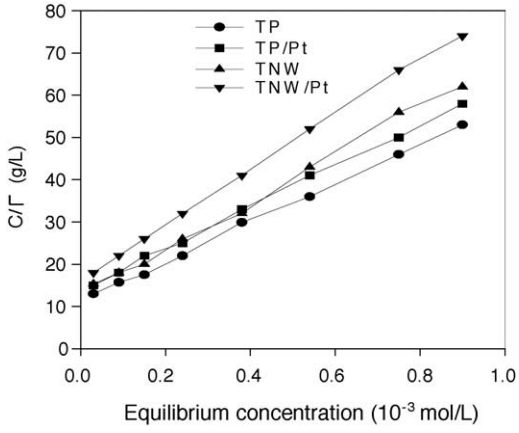


Fig. 7. The methyl orange adsorption isotherms on the different catalysts.

Table 2
The saturated adsorption capacity ($\Gamma_{max}$), the adsorption equilibrium constant ($K_a$), the apparent reaction kinetic constants ($k_{ap}$), and the kinetic constant ($k_r$) of $TiO_2$ and $TiO_2$/Pt catalysts

| Photocatalysts | $\Gamma_{max}$ ($\times 10^{-6}$ mol/g) | $K_a$ (L/mol) | $k_{ap}$ ($min^{-1}$) | $k_r$ ($\times 10^{-5}$mol/(L min)) |
|---|---|---|---|---|
| TP | 21.6 | 4100 | 0.024 | 0.58 |
| TP/Pt | 20.4 | 3528 | 0.048 | 1.35 |
| TNW | 18.0 | 4429 | 0.022 | 0.49 |
| TNW/Pt | 15.3 | 4000 | 0.038 | 0.95 |

platinised $TiO_2$ samples had a similar adsorption capacity and adsorption equilibrium constant ($K_a$) with the pure $TiO_2$ samples. Therefore, an enhancement of the photoactivity by adsorption behaviour can be excluded.

The Langmuir–Hinshelwood kinetic equation is one of the most useful models to describe this type of reaction. Usually, the Langmuir–Hinshelwood model can be simplified into the first-order model, once the substrate concentration ($C$) is very low. However, if the adsorption constant ($K_a$) is significant just like the case in this study, i.e., $K_aC$ values are significantly higher than one, the Langmuir–Hinshelwood model should not be simplified as a first order reaction, even if the substrate concentration is low. The kinetic constant ($k_{ap}$) of methyl orange photodegradations using the integrated form of the Langmuir–Hinshelwood model as follows based on the experimental data [32]:

$$L_n\left(\frac{C_0}{C}\right) + K_a(C_0 - C) = k_{ap}t \quad (10)$$

where $k_{ap} = k_rK_a$ is the apparent rate constant in $min^{-1}$, $k_r$ the photodegradation reaction rate constant in mol/(L min), $t$ the reaction time in min and $C_0$ is the initial equilibrium concentration.

The kinetic parameters ($k_{ap}$ and $k_r$) were calculated, respectively. The data as shown in Table 2 showed that the methyl orange photodegradation using platinised $TiO_2$ catalysts was remarkably enhanced. The photoreaction constant ($k_r$) of TP/Pt and TNW/Pt was 2.3 and 2 times of that of TP and TNW, respectively.

It can be explained by a quick transfer of photogenerated electrons from $TiO_2$ to the neighbour metal particles, retarding electron–hole recombination and thus raising efficiency of the oxidation power of the positive holes. Pt nanoparticles are very effective traps for the electrons due to the formation of a Schottky barrier at the metal–semiconductor contact [33]. Pt nanoparticles can be beneficial by reducing the over-potential valve for transfer of electrons to molecular oxygen and all the subsequent oxidative reaction steps in the presence of molecular oxygen. This effect allows direct oxidation of the organic compounds by holes and $HO^{\bullet}$ radicals as well. The main impact of Pt-loaded $TiO_2$ lies in a higher generation rate of oxidising species, e.g. holes or $HO^{\bullet}$ radicals than conventional heating operation.

## 4. Conclusions

A microwave assisted rapid heating method was used to prepare $TiO_2$ powder and nanowire supported Pt nanoparticles with high photocatalytic activities in the decomposition of methyl orange. The preparation method is simple, fast, and energy efficient. The Pt nanoparticles, which were uniformly dispersed on $TiO_2$ particles or nanowire, were 2–6 nm in diameters and had a very narrow particle size distribution. X-ray diffraction showed that $TiO_2$/Pt composites only displayed the characteristic diffraction peaks of a $TiO_2$ anatase structure. XPS analysis revealed that the catalysts contained mostly Pt(0), with traces of Pt(II), and Pt(IV).

The platinised $TiO_2$ samples had a similar adsorption capacity and adsorption equilibrium constant with the pure $TiO_2$ samples. Therefore, an enhancement of the photoactivity by adsorption behaviour can be excluded. An enhancement of the photocatalytic activity of platinised $TiO_2$ is attributed to a quick transfer of photogenerated electrons from $TiO_2$ to Pt nanoparticles, retarding electron–hole recombination.

## Acknowledgment

This work was financially supported by Singapore Institute of Materials Research and Engineering, Agency for Science & Technology and Research program.

## References

[1] S. Ito, T. Deguchi, K. Imai, H. Tada, Electrochem. Solid-State Lett. 2 (1999) 440.
[2] N.R. Tacconi, C.A. Boyles, K. Rajeshwar, Langmuir 16 (2000) 5665.
[3] H. Nur, S. Ikeda, B. Ohtani, Chem. Commun. (2000) 2235.
[4] S.W. Lee, W.M. Sigmund, Chem. Commun. (2003) 780.
[5] T. Kasuga, M. Hiramatsu, A. Hoson, T. Sekino, K. Niihara, Adv. Mater. 11 (1999) 1307.
[6] Y.X. Zhang, G.H. Li, Y.X. Jin, Y. Zhang, J. Zhang, L.D. Zhang, Chem. Phys. Lett. 365 (2002) 300.
[7] T. Kasuga, M. Hiramatsu, A. Hoson, T. Sekino, K. Niihara, Langmuir 14 (1998) 3160.
[8] H. Gerishe, J. Phys. Chem. 88 (1984) 6069.
[9] B. Ohtani, R.M. Bowman, D.P. Colombo, H. Kominami, H. Noguchi, K. Uosaki, Chem. Lett. (1998) 579.
[10] S. Sato, J.M. White, Chem. Phys. Lett. 72 (1980) 83.
[11] S. Sato, J.M. White, J. Phys. Chem. 85 (1981) 592.
[12] I. Izumi, F.R.F. Fan, A.J. Bard, J. Phys. Chem. 85 (1981) 218.
[13] M.R.S. John, A.J. Furgala, A.F. Sammells, J. Phys. Chem. 87 (1983) 801.
[14] D. Hufschmidt, D. Bahnemann, J.J. Testa, C.A. Emilio, M.I. Litter, J. Photochem. Photobiol., A: Chem. 148 (2002) 223.
[15] H. Einaga, M. Harada, S. Futamura, T. Ibusuki, J. Phys. Chem. B 107 (2003) 9290.
[16] W.X. Chen, J.Y. Lee, Z.L. Liu, Chem. Commun. (2002) 2588.
[17] Z.L. Liu, J.Y. Lee, W.X. Chen, M. Han, L.M. Gan, Langmuir 20 (2004) 181.
[18] A. Miyazaki, I. Balint, K.I. Aika, Y. Nakano, J. Catal. 203 (2001) 364.

[19] S.A. Galema, Chem. Soc. Rev. 26 (1997) 233.
[20] C.D. Wagner, W.M. Riggs, L.E. Davis, J.F. Moulder, in: G.E. Mullemberg (Ed.), Handbook of X-Ray Photoelectron Spectroscopy, Perkin-Elmer Corporation, Eden Prairie, MN, 1978.
[21] M.S.P. Francisco, V.R. Masterlaro, P.A.P. Nascente, A.O. Florentino, J. Phys. Chem. B 105 (2001) 10515.
[22] Z.L. Liu, X.H. Lin, J.Y. Lee, W.D. Zhang, M. Han, L.M. Gan, Langmuir 18 (2002) 4054.
[23] N.M. Rahman, K.M. Krishna, T. Soga, T. Jimbo, M. Umeno, J. Phys. Chem. Solids 60 (1999) 201.
[24] L. Biener, M. Baumer, J. Wang, R.J. Madrix, Surf. Sci. 450 (2000) 12.
[25] Q. Wang, R.J. Madrix, Surf. Sci. 474 (2001) 213.
[26] A.K. Shukla, M.K. Ravikumar, A. Roy, S.R. Barman, D.D. Sarma, A.S. Aricò, V. Antonucci, I. Pino, N. Giordano, J. Electrochem. Soc. 141 (1994) 1517.
[27] C. Roth, M. Goetz, H. Fuess, J. Appl. Electrochem. 31 (2001) 793.
[28] F. Chen, Y. Xie, J. He, J. Zhao, J. Photochem. Photobiol., A: Chem. 138 (2001) 139.
[29] Y.M. Xu, C.H. Langford, Langmuir 17 (2001) 897.
[30] C. Hu, Y. Tang, J.C. Yu, P.K. Wong, Appl. Catal., B: Environ. 40 (2003) 131.
[31] X.Z. Li, H. Liu, L.F. Cheng, H.J. Tong, Environ. Sci. Technol. 37 (2003) 3989.
[32] F.B. Li, X.Z. Li, M.F. Hou, Appl. Catal., B: Environ. 48 (2004) 185.
[33] A. Linsebigler, G. Lu, J. Yates, Chem. Rev. 95 (1995) 735.